

Temperature-dependent broadening of coherent current peaks in InAs double quantum dots

Olfa Dani,¹ Robert Hussein,² Johannes C. Bayer,¹ Sigmund Kohler,³ and Rolf J. Haug¹

¹*Institut für Festkörperphysik, Leibniz Universität Hannover, D-30167 Hannover, Germany*

²*Institut für Festkörpertheorie und -optik, Friedrich-Schiller-Universität Jena, D-07743 Jena, Germany*

³*Instituto de Ciencia de Materiales de Madrid, CSIC, E-28049 Madrid, Spain*

(Dated: April 14, 2022)

Quantum systems as used for quantum computation or quantum sensing are nowadays often realized in solid state devices as e.g. complex Josephson circuits or coupled quantum-dot systems. Condensed matter as an environment influences heavily the quantum coherence of such systems. Here, we investigate electron transport through asymmetrically coupled InAs double quantum dots and observe an extremely strong temperature dependence of the coherent current peaks of single-electron tunneling. We analyze experimentally and theoretically the broadening of such coherent current peaks up to temperatures of 20 K and we are able to model it with quantum dissipation being due to two different bosonic baths. These bosonic baths mainly originate from substrate phonons. Application of a magnetic field helps us to identify the different quantum dot states through their temperature dependence.

Introduction

The building blocks of quantum information technology and future quantum computers are qubits. Qubits can be based on coherent superpositions in double quantum dots (DQD) and such DQDs can be easily formed in a variety of semiconducting materials. The use of semiconductor technology guarantees more or less the necessary scalability of qubit structures. Along these lines it has been shown recently that qubits based on quantum dots can be formed and manipulated in CMOS technology [1] at not very low temperatures [2], i.e. quantum-dot based quantum computers seem to be within reach. The first observation of a coherent mode in a DQD system dates back more than 20 years [3], while successful coherent manipulation of electronic states [4, 5] or of spin states [6, 7] in DQDs has been shown few years later opening the path towards quantum information processing with quantum dots.

Coherence properties of a quantum state depend on the influence of the environment. Already in the early studies of DQDs it became clear that they interact with the environment via the emission of phonons [8–10]. Measurements of phonon emission were repeated in more detail just recently [11]. Whereas in these works coupling to the phonon bath has been studied in great detail for detuned quantum dots, corresponding studies just at the resonance are scarce. In addition to the mentioning of some temperature dependence of the so-called elastic peak in refs. [8, 10], a theoretical work studied phonon decoherence in 2005 [12], and it has been shown that at low temperatures electron-phonon scattering can enhance the current noise close to resonance, as has been discussed experimentally [13] and theoretically [14–16].

Here, we focus on the detailed temperature dependence of the resonant tunnel current which is mainly caused by the coupling to the phonon environment. We describe the quantum dissipation of the coherent current peaks up to temperatures of 20 K by introducing couplings to two different bosonic baths.

Experiment

For our studies we use self-assembled InAs quantum dots similar to the ones used in Refs. [13, 14] where the second quantum dot grows on top of the first dot due to strain fields induced by the InAs islands [17]. The second dot is slightly larger than

the first one [18]. AlAs layers of nominally identical thickness are used to separate the InAs quantum dots from the doped GaAs layers and from each other, as depicted in Fig. 1b. Due to the difference in size of the two quantum dots the effective thickness of the AlAs barriers is different and the coupling to the leads is asymmetric. Each characteristic feature in the measured current of our device is expected to arise from a single DQD channel although several dots are present. The line plot in Fig. 1a shows the current I through the DQD device as a function of the bias voltage V for different temperatures ranging from 1.5 K to 21 K. The graph shows two distinct current peaks at $V \approx 155$ mV (peak I) and $V \approx 187$ mV (peak II) which are due to resonant tunneling of single electrons through the InAs double quantum dots. The left peak (see also left schematic level diagram in Fig. 1a) corresponds to only a single electron being present in the DQD and originates from tunnel cycles with the occupation $(0, 0) \rightarrow (1, 0) \rightarrow (0, 1)$. This situation is depicted in the charging diagram in Fig. 1e as triple point I. The right peak in Fig. 1a corresponds to single-electron tunneling through InAs quantum dots with an additional electron being present and including double occupation, namely $(1, 0) \rightarrow (2, 0) \rightarrow (1, 1)$ (see right schematic level diagram in Fig. 1a and triple point II in the charging diagram in Fig. 1e). Even though in a simplified understanding of single-electron tunneling through DQDs, the tunnel resonances should not be affected by the Fermi distributions in the leads due to the low temperatures and the resonances being far away from the Fermi levels in the leads, we observe quite a strong temperature dependence of both the amplitude and the width of both peaks in Fig. 1a. With increasing temperature, the current resonances significantly broaden and at the same time the amplitude of the peaks decreases. Both effects are accompanied by a shift of the peak position toward slightly more positive voltages. This shift is attributed to temperature-dependent changes in the electric field distribution in the sample.

Whilst both resonances show similar behaviour as function of temperature, the magnetic field dependence reveals major differences. The colour graphs in Fig. 1c,d show the current of the respective resonance as function of bias voltage and magnetic field up to $B = 2$ T at $T = 1.5$ K. For peak I, the

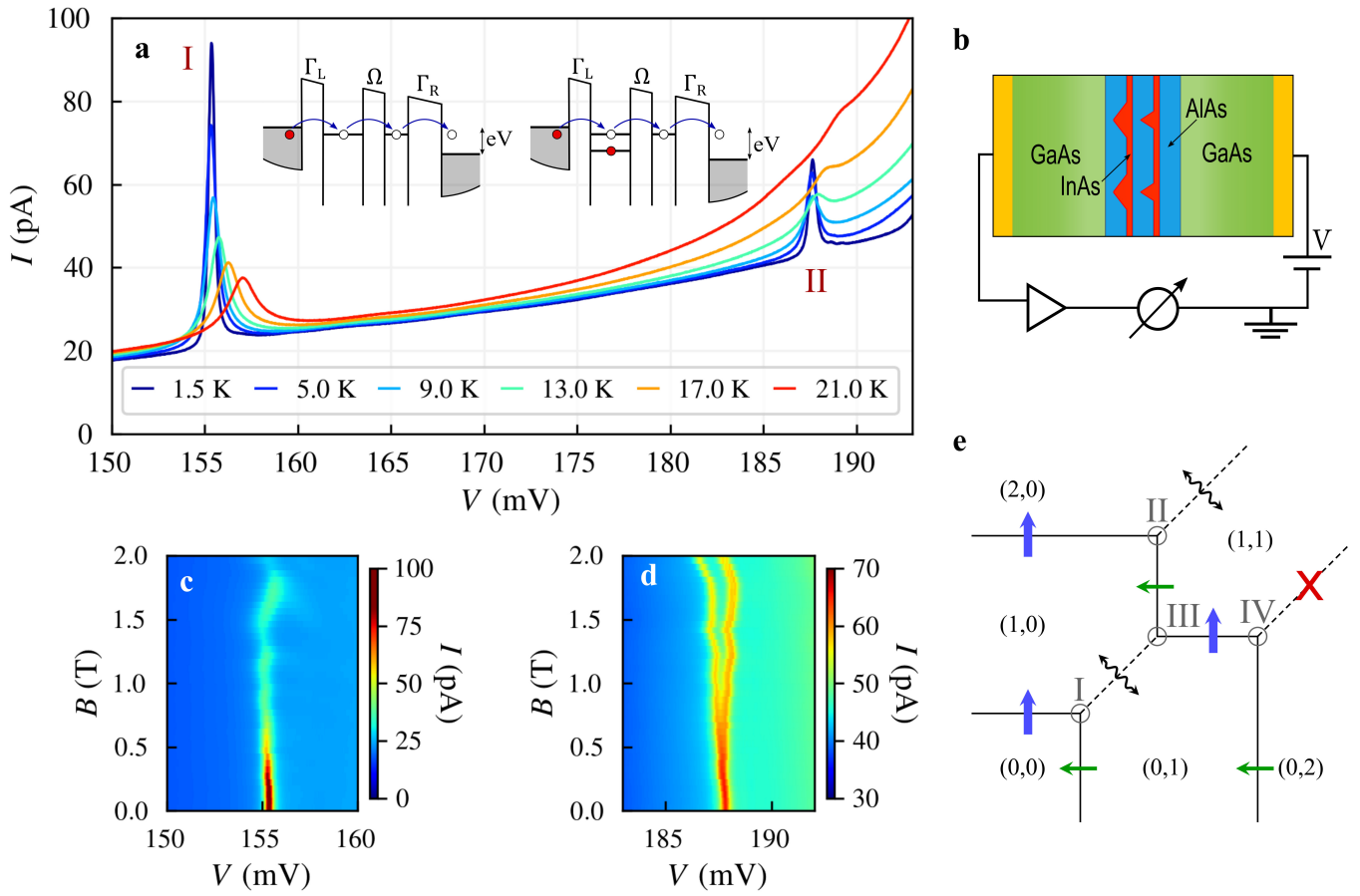


FIG. 1. Experiment. **a**, Current-voltage characteristic of InAs double quantum dots (DQDs) for different temperatures between 1.5 and 21 K. The inset shows simplified energy level diagrams of the DQD system: the left diagram for the first resonance peak (peak I) around 155 mV and the right diagram for the second resonance peak (peak II) around 188 mV. **b**, Schematic image of the investigated heterostructure and the measurement set-up, see methods section for detailed information. **c**, Current of resonance I as function of voltage and magnetic field at $T = 1.5$ K. **d**, Same for resonance II. **e**, Charging diagram of the double quantum dot system with all the triple points involving one and two electron states. The different couplings to the two leads are depicted by arrows with different colours and thicknesses.

main effect of the magnetic field seems to be a reduction of the peak amplitude. The magnetic field was applied perpendicular to the layer structure and parallel to the current. Therefore the weak oscillation observed for the magnetic field dependence of the resonances originates from the Landau-level structure in the emitter. For peak II (Fig. 1d), not only is the amplitude much less affected in comparison to the first peak, but the single resonance splits into two. This indicates that the two peaks emerge from different electron configurations, where the left peak I corresponds to a single-electron triple point, whereas the right peak II involves a double occupation of the larger quantum dot. In the charging diagram in Fig. 1e two more triple points appear which are not expected to be observable in our structure. Triple point IV will be spin blocked, whereas triple point III corresponds to hole like transport which exchanges the role of the asymmetric couplings and therefore, these current peaks will be much smaller.

For now, we want to focus on the temperature dependence of the resonances. However, not only the peaks in the current are influenced by increasing temperature, also the off-resonant

background current experiences a temperature dependent increase. Especially for the right peak II and the highest temperatures the increasing background current interferes with the appearance and the visibility of the resonance peak. In order to analyse the current resonances in more detail, we subtracted this temperature-dependent background and will discuss it later. In Fig. 2 the current resonances are presented after subtraction of the background current and after normalizing to the peak position. For three temperatures, peak I is presented in Fig. 2a, whereas in Fig. 2b peak II is shown. For both peaks one sees a clear decrease in amplitude and increase in broadening with temperature.

Theoretical model

For a theoretical description, we model each quantum dot as a single orbital with energy ϵ_ℓ ($\ell = L, R$) and tunnel coupling Ω . For states with more than one electron, we consider the onsite and nearest-neighbour interaction energies U and U' , respectively. Each dot is tunnel coupled also to a lead which enables electron transitions with the rates Γ_ℓ from lead $\ell = L, R$ to the dot and back, depending on the Fermi energy of

the respective lead. For sufficiently small tunnel coupling, the leads are eliminated within a Bloch-Redfield approach [19, 20] which leads to a master equation for the reduced density operator of the DQD in a many-body basis [21]. Here, the relatively small inter-dot tunneling in the experiment requires us to work beyond a secular approximation, i.e., to take off-diagonal density matrix elements into account. For a detailed description of the formalism, see the Supplementary Material [22].

Quantum dissipation is modeled by a coupling to bosonic environmental degrees of freedom with the Hamiltonian $H_{\text{el-env}} = Z\xi$ with the (dimensionless) DQD dipole operator $Z = n_L - n_R$ and $n_\ell = 0, 1, 2$ the occupation of dot ℓ , as sketched in Fig. 2c. The quantum noise $\xi = \sum_\nu \lambda_\nu (a_\nu^\dagger + a_\nu)$ originates from bosonic modes ν with frequency ω_ν , annihilation operator a_ν , and coupling strength λ_ν [23–26]. We assume the modes to be initially at thermal equilibrium with temperature T . The corresponding rates for dissipation and decoherence can be expressed in terms of the spectral density $J(\omega) = \pi \sum_\nu |\lambda_\nu|^2 \delta(\omega - \omega_\nu) \equiv \pi\alpha\omega/2$, which we assume to be Ohmic, i.e., linear in the frequency ω . A particular role is played by the dimensionless dissipation strength α which determines the magnitude of dissipation and decoherence. One of our main goals is to determine α from experimental data. Let us remark that the DQD-bath model has been chosen such that for the DQD occupation with a single electron, the tunnel term in H_{DQD} and the coupling operator Z can be represented by the Pauli matrices σ_x and σ_z , respectively. Then our Hamiltonian becomes the usual Caldeira-Leggett model [23–25] $H = \frac{\Omega}{2}\sigma_x + \frac{\epsilon}{2}\sigma_z + \sigma_z\xi$ for the dissipative two-level system with detuning $\epsilon = \epsilon_L - \epsilon_R$. It undergoes a phase transition at $\alpha = 1$, while for $\alpha \ll 1$, its dynamics is governed by quantum coherence.

For a strong detuning of the DQD levels, the dipole operator Z is practically a good quantum number, i.e., it approximately commutes with the DQD Hamiltonian and, thus, cannot cause significant transitions. Therefore, as we will see in our numerical results, $H_{\text{el-env}}$ may explain the broadening of the peaks, but not the emergence of the temperature dependent background. To model also the latter, we introduce a second heat bath with the Hamiltonian $H'_{\text{el-env}} = X \sum_\nu \lambda_\nu (b_\nu^\dagger + b_\nu)$, where the annihilation operator b_ν , the spectral density, and the dimensionless dissipation strength α' are defined as for the first bath. The coupling is established via the tunnel operator $X = \sum_\sigma (c_{L\sigma}^\dagger c_{R\sigma} + c_{R\sigma}^\dagger c_{L\sigma})$ and, thus, can induce dissipative transitions of electrons from one QD to the other. Hence, this bath is relevant mainly when the DQD eigenstates are localized, i.e., far from the peaks where the detuning dominates. Physically, this corresponds to coupling the intra-dot current to an environment.

Peak broadening

The most significant observation in the measured current peaks is their broadening with increasing temperature. After subtraction of the background the peaks reveal a Lorentzian shape, see Fig. 2a,b. In panel b, we also witness that with increasing temperature, the Lorentzian may be distorted by small resonances in its vicinity. Our first goal is to determine the tunnel

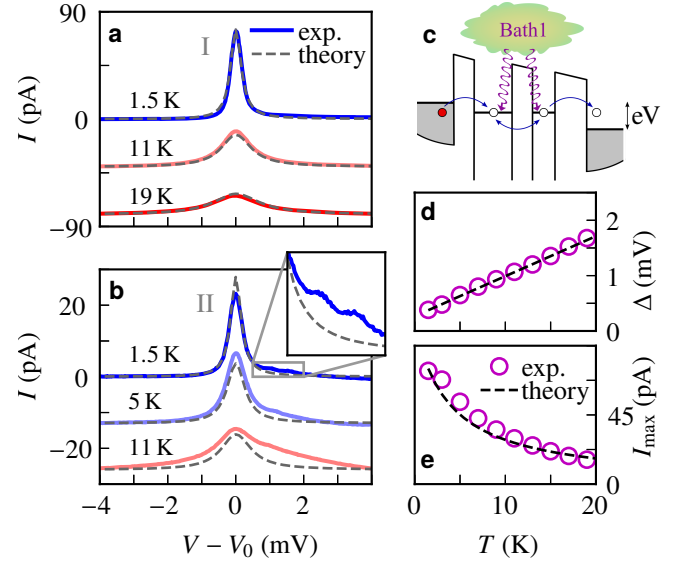


FIG. 2. Analysis of the current peaks. **a,b**, Enlargement of the measured peaks at $V_0 \approx 155$ mV (peak I) and $V_0 \approx 188$ mV (peak II), respectively, with the background subtracted (solid lines) in comparison with the result of the theoretical prediction with only bath 1 (dashed) for various temperatures. The inset of panel b reveals the presence of two further resonances. **c**, Corresponding model with an environment coupled to the difference of the onsite energies. **d,e**, Width Δ and height I_{max} of peak I in dependence of the temperature. Experimental values are depicted by circles while the dotted line shows the current of the full model with $\Gamma_L = 500 \mu\text{eV}$, $\Gamma_R = 30 \mu\text{eV}$, $\Omega = 4 \mu\text{eV}$, $\alpha = 0.011$, and $\alpha' = 0$.

couplings $\Gamma_{L,R}$ and Ω as well as the dimensionless dissipation strength α . Without the background, it turns out to be sufficient to consider only bath 1. The task is facilitated by the approximate solution for the current

$$I \approx \frac{e}{\hbar} \frac{\Omega^2 (\gamma - 2\pi\alpha\epsilon)}{4\epsilon^2 + (\gamma + 2\Omega^2/\Gamma_R)\gamma} \quad (1)$$

with $\gamma = \Gamma_R + 4\pi\alpha k_B T$ and the detuning $\epsilon = \eta e(V - V_{\text{peak}})$ with the peak position V_{peak} and the leverage $\eta = 0.15$. For a derivation, see the Supplementary Material [22]. Then for the relatively large temperatures in our experiment, the peak as a function of the detuning ϵ has the width γ , while its height reads $e\Omega^2/\hbar\gamma$. Hence, from the linear behavior of the width of peak I as a function of T (Fig. 2d), we can immediately read off $\Gamma_R = 30 \mu\text{eV}$ and $\alpha = 0.011$. With these parameters at hand, the peak height shown in Fig. 2e provides the inter-dot tunneling $\Omega = 4.2 \mu\text{eV}$. Quite remarkably, the tunneling from the emitter, Γ_L , is of minor relevance, as long as $\Gamma_L \gg \Gamma_R$ showing the dominance of the smallest rate in tunneling. Using these values, the theoretical results for the shape of the peaks agrees rather well with the experimental data.

For peak II, the determination of the width at high temperatures is hindered by the emergence of two small, but close peaks visible in the inset of Fig. 2b. Nevertheless, we find that the above values for Γ_L and α predict also the width of this peak. However, matching the peak height requires a significantly smaller inter-dot tunneling $\Omega = 1.8 \mu\text{eV}$. Therefore, we

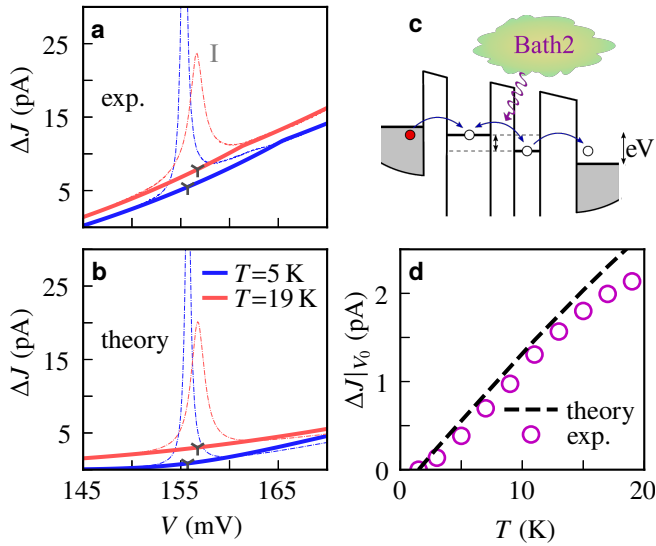


FIG. 3. Analysis of the background. **a**, Measured tunneling current for the first peak for three different temperatures (thin black lines) and subtracted background (coloured lines). **b**, Corresponding theoretical results. **c**, Sketch of the coupling of the tunnel operator to bath 2 which causes a smooth background current. **d**, shift of the current baseline from its value at 1.5 K in dependence of the temperature, ΔJ , at the peak position. The theoretical values are computed with $\alpha' = 2.4 \cdot 10^{-6}$, while all other parameters are as in Fig. 2.

conclude that the two peaks investigated stem from different DQDs.

Background

We have seen that the coupling to a heat bath via the DQD dipole moment can provide a faithful description of the broadening of the resonance peaks. However, it does not explain the smooth, temperature-dependent background witnessed in the experimental data shown in Fig. 1a and detailed in Fig. 3a. We attribute this background to a weak coupling of the inter-dot current to an environment modeled by our second bath. In the following we estimate the corresponding dissipation strength α' . To compensate the impact of other double dots in our sample, we focus on how the baseline of the peak raises from its value at the lowest temperature used in the experiment, 1.5 K, which provides the data in Fig. 3d. For the theoretical analysis, we now include also the dissipative inter-dot tunneling sketched in Fig. 3c.

For the fitting, we again start with an analytic estimate. In doing so, we derive with a standard calculation [22] the dissipative transition rate between the states $(1, 0)$ and $(0, 1)$, which reads $\kappa(\epsilon) = \pi\alpha'\epsilon/\hbar(1 - e^{-\epsilon/kT})$. Since these dissipative transitions are rather slow, they represent the bottleneck of the transport and determine the current such that $I \sim e\gamma(\epsilon)$. For the dissipation strength $\alpha' = 2.4 \cdot 10^{-6}$, the theory result for ΔJ agrees with our experimental data. Remarkably, already for $\alpha' \sim 10^{-4}\alpha$, the second bath has a significant influence. This is in agreement with previous theoretical findings [27] that a heat bath that couples via the tunnel operator may have a rather strong impact already for small values of α' .

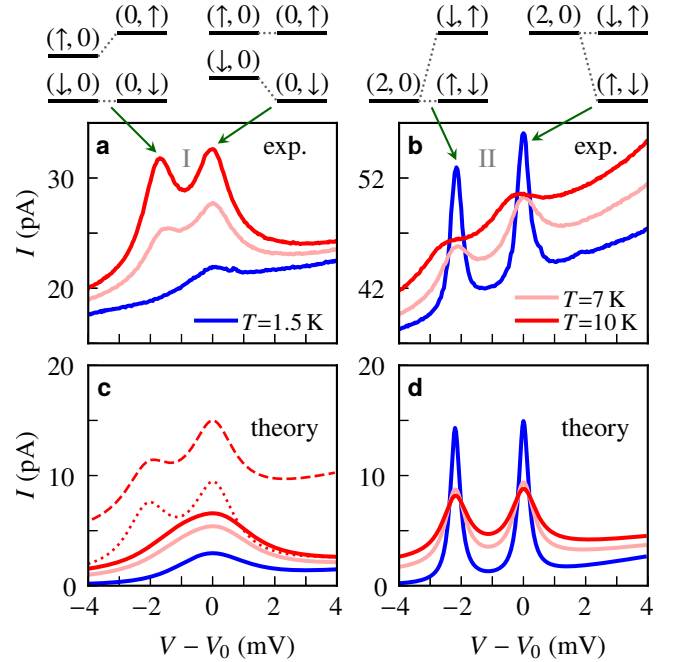


FIG. 4. Influence of a magnetic field. **a,b**, Temperature dependence of the current peaks at 155 mV (a) and 188 mV (b) in a magnetic field with $B = 4$ T. The level schemes on top sketch the resonant processes that lead to the peaks as is explained in the text. **c,d**, The theory curves computed with the inhomogeneity $\Delta E_Z = 0.33$ meV, such that for $\eta = 0.15$ the peaks are separated by 2.2 mV. All other parameters are as in Fig. 3. The additional lines in panel c are computed with a significantly larger $\alpha' = 10^{-5}$ (dashed line) and with additional spin flips (dotted, for details see the Supplementary Material [22]).

The comparison of the theoretically computed background in Fig. 3b exhibit a qualitative agreement with experimental data. On a quantitative level, however, the shape of the background is reproduced by the model not as well as the peak itself. One reason for this is that the impact of neighboring DQDs cannot be isolated with sufficient precision. Another reason is that in contrast to bath 1, the present dissipative decay probes the spectral density of the bath in a broad frequency range. Therefore, the assumption of an Ohmic monotonic spectral density naturally implies limited agreement [11]. Nevertheless, our model is capable of explaining the physics that leads to the background of the current peaks.

Zeeman splitting

Both current peaks analyzed above may be fitted with either a one-electron model or with a model with up to two electrons. However, as indicated in Fig. 1c,d, both lead to different behavior in the presence of a magnetic field. Specifically, peak II splits up, while peak I does not, at least not at 1.5 K. To analyze the impact of a magnetic field in more detail, we add a Zeeman term to our model and elaborate the resulting temperature dependence of the peaks.

While in our experiment, the magnetic field is homogeneous, the g -factors of the dots are different due to the different sizes of the two dots and such the Zeeman splitting becomes inhomogeneous. With the observed splitting of $\Delta V_Z = 2.2$ mV

at $B = 4$ T, and the leverage factor $\eta = 0.15$, we calculate $\Delta g = 1.42$, which seems reasonable in comparison to single dot devices of similar size [28]. The details of the individual g -factors are not observed in our experiment. We use in our model as parameters the average Zeeman energy \bar{E}_Z and their difference ΔE_Z . Provided that the Zeeman splitting does not shift any energy level across the Fermi surface, \bar{E}_Z has no relevant influence. Hence, an appropriate extension of the model can be described by the Hamiltonian $H_{\text{Zeeman}} = \frac{1}{2}\Delta E_Z(n_{L\downarrow} - n_{L\uparrow} - n_{R\uparrow} + n_{R\downarrow})$, where ΔE_Z is determined from the splitting of the peak.

Figure 4 depicts the corresponding measured (panels a and b) and computed (panels c and d) current peaks for various temperatures. As already seen in Fig. 1b, at $T = 1.5$ K we witness a single peak, while Fig. 4a shows that with increasing temperature, a second peak emerges. This observation can be explained with the level scheme sketched on top of the experimental plots. For an inhomogeneous Zeeman splitting, the transport channels cannot be resonant at the same time. Hence, an electron may get stuck in the off-resonant channel and block transport. However, owing to the coupling to the bath, a dissipative decay $(\downarrow, 0) \rightarrow (0, \downarrow)$ can resolve the blockade such that a current can flow. For the spin-up channel, however, the corresponding process requires the absorption of energy from the bath and, therefore, can occur only at sufficiently high temperatures. The results obtained with our theoretical model qualitatively explain the emergence of the second peak in the temperature regime of the experiment. In the numerical data, however, the second peak is poorly resolved, as only a small shoulder emerges. For this discrepancy between theory and experiment two possible reasons come to mind. First, the magnetic field may distort the electron wave function such that the dissipation strength α' becomes larger and, thus, dissipation-assisted tunneling is enhanced. The dashed line in Fig. 4c shows with larger α' indeed a double peak emerges. A further possible explanation is that with increasing Zeeman splitting, spin flips play a more important role. Then an electron in the blocked channel can undergo a spin flip and, thus, end up in the resonant channel. The dotted line in panel c demonstrates that also this conjecture leads to a double peak (details of the corresponding model are given the Supplementary Material [22]).

For peak II, this kind of current blockade does not occur, because the resonant state in the left QD is the spin singlet $(\uparrow\downarrow, 0)$ which is unaffected by the magnetic field. Hence, we observe a double peak also at low temperatures. With increasing temperature, each peak broadens much like the single peaks obtained in the absence of a magnetic field.

Discussion and conclusions

We have measured resonance peaks in the current through InAs double quantum dots and showed how their width and background increase with temperature in the range of 1.5–21 K. This behavior can be fully explained by introducing

two (bosonic) baths of the Caldeira-Leggett type. The peak broadening can be modeled with rather good precision with a bath that couples via the dipole moment of the DQD. Far from the peak, however, this bath has little influence. Therefore, we introduced a second bath that couples to the DQD current which in a tight-binding description is given by the tunnel operator. We determined the corresponding dimensionless dissipation strength of each bath. Physically, the baths describe the influence of substrate phonons and also of the impedance of the electromagnetic environment [29, 30].

A magnetic field makes the situation more complex. In particular, we found that then the behavior of the peaks depends on the triple point at which the DQD is operated. In turn, this allows one to determine whether two-electron states play a role.

The interest in the dissipative model parameters extends beyond the description of current peaks. For example, with the dot-lead couplings suppressed, the one-electron states form a charge qubit whose dephasing time as a function of the dissipation strength is determined by the corresponding rates in the quantum master equation (see the Supplementary Material [22]) and in the absence of the second bath is known analytically [26, 31]. In the temperature regime of the experiment the present values of α and α' correspond to a dephasing time of the order $T_2 \sim 100$ ps, where the precise value depends also on the detuning. Assuming that the same model parameters are valid at lower temperatures, one can predict coherence times up to 10 ns. Therefore, our analysis allows us to predict parameters being essential for all approaches involving manipulation of quantum states.

Acknowledgements

O.D., J.C.B., and R.J.H. acknowledge funding by the Deutsche Forschungsgemeinschaft (DFG, German Research Foundation) under Germany's Excellence Strategy -EXC 2123 QuantumFrontiers-390837967 and the State of Lower Saxony of Germany via the Hannover School for Nanotechnology. S.K. acknowledges financial support by the Spanish Ministry of Science and Innovation through Grant. No. PID2020-117787GB-I00 and the CSIC Research Platform on Quantum Technologies PTI-001. The authors thank Jan Kühne and Felix Opiela for contributions at the beginning of the project.

Author contributions

O.D. and J.C.B. performed the measurements and the analysis of the experimental data. R.H. and S.K. developed the theoretical model and computed the numerical data. All authors participated in the discussions of the results and contributed to the writing and editing the manuscript. The research was supervised by S.K. and R.J.H.

Competing interests

The authors declare no competing interests.

[1] X. Xue, B. Patra, J. P. G. van Dijk, N. Samkharadze, S. Subramanian, A. Corna, B. Paquelet Wuetz, C. Jeon, F. Sheikh,

E. Juarez-Hernandez, B. P. Esparza, H. Rampurawala, B. Carl-

- ton, S. Ravikumar, C. Nieva, S. Kim, H.-J. Lee, A. Sammak, G. Scappucci, M. Veldhorst, F. Sebastiano, M. Babaie, S. Pellerano, E. Charbon, and L. M. K. Vandersypen, CMOS-based cryogenic control of silicon quantum circuits, *Nature* **593**, 205 (2021).
- [2] C. H. Yang, R. C. C. Leon, J. C. C. Hwang, A. Saraiva, T. Tanttu, W. Huang, J. Camirand Lemyre, K. W. Chan, K. Y. Tan, F. E. Hudson, K. M. Itoh, A. Morello, M. Pioro-Ladrière, A. Laucht, and A. S. Dzurak, Operation of a silicon quantum processor unit cell above one kelvin, *Nature* **580**, 350 (2020).
- [3] R. H. Blick, D. Pfannkuche, R. J. Haug, K. v. Klitzing, and K. Eberl, Formation of a Coherent Mode in a Double Quantum Dot, *Phys. Rev. Lett.* **80**, 4032 (1998).
- [4] T. Hayashi, T. Fujisawa, H. D. Cheong, Y. H. Jeong, and Y. Hira-yama, Coherent Manipulation of Electronic States in a Double Quantum Dot, *Phys. Rev. Lett.* **91**, 226804 (2003).
- [5] J. R. Petta, A. C. Johnson, C. M. Marcus, M. P. Hanson, and A. C. Gossard, Manipulation of a Single Charge in a Double Quantum Dot, *Phys. Rev. Lett.* **93**, 186802 (2004).
- [6] F. H. L. Koppens, J. A. Folk, J. M. Elzerman, R. Hanson, L. H. Willems van Beveren, I. T. Vink, H. P. Tranitz, W. Wegscheider, L. P. Kouwenhoven, and L. M. K. Vandersypen, Control and Detection of Singlet-Triplet Mixing in a Random Nuclear Field, *Science* **309**, 1346 (2005).
- [7] J. R. Petta, A. C. Johnson, J. M. Taylor, E. A. Laird, A. Ya-coby, M. D. Lukin, C. M. Marcus, M. P. Hanson, and A. C. Gossard, Coherent Manipulation of Coupled Electron Spins in Semiconductor Quantum Dots, *Science* **309**, 2180 (2005).
- [8] T. Fujisawa, T. H. Oosterkamp, W. G. van der Wiel, B. W. Broer, R. Aguado, S. Tarucha, and L. P. Kouwenhoven, Spontaneous Emission Spectrum in Double Quantum Dot Devices, *Science* **282**, 932 (1998).
- [9] T. Brandes and B. Kramer, Spontaneous Emission of Phonons by Coupled Quantum Dots, *Phys. Rev. Lett.* **83**, 3021 (1999).
- [10] W. G. van der Wiel, S. De Franceschi, J. M. Elzerman, T. Fujisawa, S. Tarucha, and L. P. Kouwenhoven, Electron transport through double quantum dots, *Rev. Mod. Phys.* **75**, 1 (2002).
- [11] A. Hofmann, C. Karlewski, A. Heimes, C. Reichl, W. Wegscheider, G. Schön, K. Ensslin, T. Ihn, and V. F. Maisi, Phonon spectral density in a GaAs/AlGaAs double quantum dot, *Phys. Rev. Research* **2**, 033230 (2020).
- [12] S. Vorojtsov, E. R. Mucciolo, and H. U. Baranger, Phonon decoherence of a double quantum dot charge qubit, *Phys. Rev. B* **71**, 205322 (2005).
- [13] P. Barthold, F. Hohls, N. Maire, K. Pierz, and R. J. Haug, Enhanced Shot Noise in Tunneling through a Stack of Coupled Quantum Dots, *Phys. Rev. Lett.* **96**, 246804 (2006).
- [14] G. Kießlich, E. Schöll, T. Brandes, F. Hohls, and R. J. Haug, Noise Enhancement due to Quantum Coherence in Coupled Quantum Dots, *Phys. Rev. Lett.* **99**, 206602 (2007).
- [15] A. Braggio, C. Flindt, and T. Novotný, Non-Markovian signatures in the current noise of a charge qubit, *Physica E* **40**, 1745 (2008).
- [16] R. Sánchez, S. Kohler, P. Hänggi, and G. Platero, Electron bunching in stacks of coupled quantum dots, *Phys. Rev. B* **77**, 035409 (2008).
- [17] Q. Xie, A. Madhukar, P. Chen, and N. P. Kobayashi, Vertically Self-Organized InAs Quantum Box Islands on GaAs(100), *Phys. Rev. Lett.* **75**, 2542 (1995).
- [18] H. Eisele, O. Flebbe, T. Kalka, C. Preinesberger, F. Heinrichsdorff, A. Krost, D. Bimberg, and M. Dähne-Prietsch, Cross-sectional scanning-tunneling microscopy of stacked InAs quantum dots, *Appl. Phys. Lett.* **75**, 106 (1999).
- [19] A. G. Redfield, On the Theory of Relaxation Processes, *IBM J. Res. Develop.* **1**, 19 (1957).
- [20] H.-P. Breuer and F. Petruccione, *Theory of open quantum systems* (Oxford University Press, Oxford, 2003).
- [21] M. Stark and S. Kohler, Coherent quantum ratchets driven by tunnel oscillations, *Europhys. Lett.* **91**, 20007 (2010).
- [22] See Supplemental Material.
- [23] A. J. Leggett, S. Chakravarty, A. T. Dorsey, M. P. A. Fisher, A. Garg, and W. Zwerger, Dynamics of the dissipative two-state system, *Rev. Mod. Phys.* **59**, 1 (1987).
- [24] P. Hänggi, P. Talkner, and M. Borkovec, Reaction-rate theory: fifty years after Kramers, *Rev. Mod. Phys.* **62**, 251 (1990).
- [25] U. Weiss, *Quantum Dissipative Systems*, 2nd ed. (World Scientific, Singapore, 1998).
- [26] Y. Makhlin, G. Schön, and A. Shnirman, Quantum-state engineering with Josephson-junction devices, *Rev. Mod. Phys.* **73**, 357 (2001).
- [27] M. Bello, G. Platero, and S. Kohler, Doublon lifetimes in dissipative environments, *Phys. Rev. B* **96**, 045408 (2017).
- [28] I. Hapke-Wurst, U. Zeitler, R. J. Haug, and K. Pierz, Mapping the g factor anisotropy of InAs self-assembled quantum dots, *Physica E* **12**, 802 (2002).
- [29] M. H. Devoret, D. Esteve, H. Grabert, G.-L. Ingold, H. Pothier, and C. Urbina, Effect of the electromagnetic environment on the Coulomb blockade in ultrasmall tunnel junctions, *Phys. Rev. Lett.* **64**, 1824 (1990).
- [30] G.-L. Ingold and Yu. V. Nazarov, Charge Tunneling Rates in Ultrasmall Junctions, in *Single Charge Tunneling*, NATO ASI Series B, Vol. 294, edited by H. Grabert and M. H. Devoret (Plenum, New York, 1992) p. 21.
- [31] U. Weiss and M. Wollensak, Dynamics of the biased two-level system in metals, *Phys. Rev. Lett.* **62**, 1663 (1989).
- [32] D. Darau, G. Begemann, A. Donarini, and M. Grifoni, Interference effects on the transport characteristics of a benzene single-electron transistor, *Phys. Rev. B* **79**, 235404 (2009).
- [33] R. Hussein, S. Kohler, J. C. Bayer, T. Wagner, and R. J. Haug, Spectral Properties of Stochastic Resonance in Quantum Transport, *Phys. Rev. Lett.* **125**, 206801 (2020).
- [34] D. Weinmann, W. Häusler, and B. Kramer, Spin Blockades in Linear and Nonlinear Transport through Quantum Dots, *Phys. Rev. Lett.* **74**, 984 (1995).
- [35] K. Ono, G. Austing D., Y. Tokura, and S. Tarucha, Current Rectification by Pauli Exclusion in a Weakly Coupled Double Quantum Dot System, *Science* **297**, 1313 (2002).
- [36] D. P. DiVincenzo and D. Loss, Rigorous Born approximation and beyond for the spin-boson model, *Phys. Rev. B* **71**, 035318 (2005).

Methods

Experiment. The experimental device consists of self-assembled InAs double quantum dots, stacked between GaAs leads with annealed metal contacts. Three AlAs layers of nominally identical thickness 5 nm are used to separate the two InAs quantum dot layers from the (doped) GaAs leads and from each other. Temperature and magnetic field control were achieved by placing the device into a He4 cryostat with variable temperature insert. For all measurements, the bias voltage was applied to the contact closer to the layer of smaller QDs (right). The contact closer to the larger QDs (left) was connected to a current preamplifier ($1 \times 10^{-10} \text{ A V}^{-1}$) to ensure high sensitivity. Each datapoint was obtained by integrating the voltage output of the current preamplifier over one power

line cycle (20 ms).

Bloch-Redfield master equation. The full model Hamiltonian for the DQD and its environment is of the structure $H = H_{\text{DQD}} + H_{\text{env}} + V$, where H_{env} and the DQD-environment coupling V contain a summation over all heat baths and leads. The dynamics of the total density operator is governed by the Liouville-von Neumann equation $\dot{\rho}_{\text{tot}} = -i[H, \rho_{\text{tot}}]$ which is practically intractable owing to its macroscopic number of degrees of freedom. Therefore, we derive a master equation for the density operator of the DQD by integrating out the environment within second-order perturbation theory, which in units with $\hbar = 1$ reads [19–21]

$$\dot{\rho} = -i[H_{\text{DQD}}, \rho] - \int_0^\infty d\tau \text{tr}_{\text{env}} [V, [V(-\tau), \rho \otimes \rho_{\text{env}}]], \quad (2)$$

where $V(t) = e^{i(H_{\text{DQD}} + H_{\text{env}})t} V e^{-i(H_{\text{DQD}} + H_{\text{env}})t}$ is the coupling operator in the interaction picture and tr_{env} the trace over all bath and lead variables. Generally, Eq. (2) possesses a unique stationary solution which allows us to compute the current.

The numerical solution of the master equation is conveniently performed in the energy eigenbasis of the DQD with the many-body eigenstates $|k\rangle$ and the corresponding energies E_k and occupation numbers N_k . The main advantage of this representation is that it brings $V(t)$ to a simple form such that the time integration in Eq. (2) can be evaluated analytically. The direct transitions between the populations are determined by golden-rule rates. For example, tunneling of an electron from a lead to the DQD occurs with a rate $\Gamma_{kl}^{(\text{in})} \propto f(E_f - E_i - \mu)$ with f being the Fermi function and E_i and E_f the energies of the initial and final DQD state, whose difference must be compensated by the energy of the incoming lead electron. Hence, these terms can occur only when $E_f \lesssim E_i + \mu$. In turn, $\Gamma_{kl}^{(\text{out})} \propto f(E_f - E_i + \mu)$, which differs from $\Gamma^{(\text{in})}$ only by the sign of the chemical potential. For the dissipative transitions, one finds absorption and emission rates which are linked by Boltzmann factors.

Importantly, owing to the relatively small inter-dot tunneling in our system, off-diagonal density matrix elements are rather relevant. Indeed, one observes that ρ eventually becomes block diagonal in the occupation number N_k , where the blocks correspond to subspaces with equal DQD occupation [32]. Within these blocks, however, off-diagonal density matrix elements may have an appreciable size, which implies that a secular approximation is suitable only for pairs of states with different occupation number.

TABLE I. Parameters for the theory data shown in Fig. S1. The emitter-DQD rate, $\Gamma_L = 0.5$ meV, is the same as in the main text.

Figure	Type of TP	Ω	Γ_R	α	α'
S1a	I	$1.4 \mu\text{eV}$	$60 \mu\text{eV}$	0.007	$2.2 \cdot 10^{-6}$
S1b	II	$0.7 \mu\text{eV}$	$12 \mu\text{eV}$	0.014	$2.2 \cdot 10^{-6}$

Supplemental Material

I. Additional data

In Fig. S1, we show experimental data together with theory results for two peaks measured with a different sample of the similar layer structure. The only difference in the layer structure is a slightly increased thickness (7 nm) of the AlAs barrier layer separating the two InAs dot layers. All other measurement conditions were kept identical to the data discussed in the main text. In the presence of a magnetic field at 1.5 K (not shown), only the peak in panel b splits and, thus, the corresponding triple point must be of type II. By contrast, the behavior of the peak in Fig. S1a indicates a triple point of type I. The widths and heights of the peaks can be appreciated in Figs. S1c,d,e. For temperatures up to 10 K, they are well reproduced by our theory. For larger temperatures, the peaks become very small, such that height and width cannot be determined with sufficient precision.

II. Data analysis

The data analysis relies on the assumption that the background left and right to a resonance peak of the experimental current-voltage characteristics is growing exponentially. Their slopes are, however, distinct. It consists of (i) the subtraction of the left and right background from the raw data and (ii) the simultaneous fitting of the extracted data for different temperatures with the formula given in Eq. (1) of the main text.

In step (i), we first estimate the position and line width of the resonance in order to separate the voltage regimes relevant for the left and right background. Then, we determine their exponential regressions. Finally, we identify their intersection at which we stitch both backgrounds together. The combined background is then subtracted from the measured current-voltage characteristics. This scheme is applied to all discussed datasets and for each temperature. For a fixed dataset, we fit the extracted current-voltage characteristics simultaneously for different temperatures using averaged parameters from individual fits as initial guess. The resulting fitting parameters serve as starting point for the theoretical description incorporating the spin as discussed in the following section.

III. Three-level approximation

In refs. [14, 16], a similar model has been used, but without taking the spin degree of freedom into account. Then in

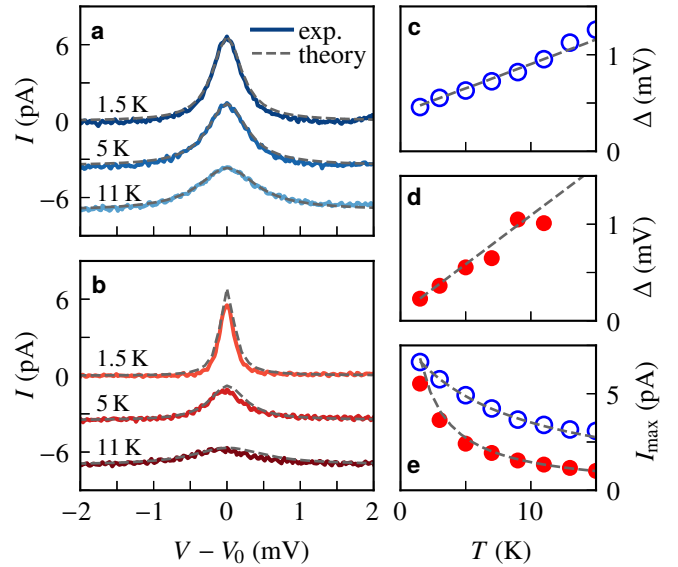


FIG. S1. (a,b) Current peaks measured at a further sample for various temperatures. (c,d,e) Corresponding peak widths and heights plotted with the respective colour. The dashed lines are theory data for the parameters summarized in Table I.

the limit of strong interaction, double occupancy is energetically forbidden and the master equation possesses an analytic solution. Our goal is now to approximate our model in the vicinities of triple points by a three-level model and to show that the resulting Liouvillian can be approximated by the one for spinless electrons. In doing so, we obtain an approximative analytical solution which facilitates parameter fitting.

A. Analytical solution for spinless electrons

When disregarding spin and double occupation, the DQD Hamiltonian can be decomposed into the basis states $|0\rangle$, $|L\rangle$, $|R\rangle$, which refer to the empty DQD and the occupation with one electron on the left and the right dot, respectively. Since in the stationary limit, coherences between the state $|0\rangle$ and the one-electron states vanish, the DQD density operator can be written in the basis of the populations p_0 , p_L , and p_R , together with the coherences ρ_{LR} and ρ_{RL} . The corresponding Liouvillian reads [16]

$$\mathcal{L} = \begin{pmatrix} -\tilde{\Gamma}_{\text{in}} & 0 & \tilde{\Gamma}_{\text{out}} & 0 & 0 \\ \tilde{\Gamma}_{\text{in}} & 0 & 0 & -\frac{i}{2}\tilde{\Omega} & \frac{i}{2}\tilde{\Omega} \\ 0 & 0 & -\tilde{\Gamma}_{\text{out}} & \frac{i}{2}\tilde{\Omega} & -\frac{i}{2}\tilde{\Omega} \\ 0 & -\frac{i}{2}\tilde{\Omega} + A_+ & \frac{i}{2}\tilde{\Omega} - A_- & i\tilde{\epsilon} - B & 0 \\ 0 & \frac{i}{2}\tilde{\Omega} + A_+ & -\frac{i}{2}\tilde{\Omega} - A_- & 0 & -i\tilde{\epsilon} - B \end{pmatrix}, \quad (3)$$

where

$$A_{\pm} = \frac{\pi}{2}\tilde{\alpha}\tilde{\Omega} \pm \frac{\pi}{2}\tilde{\alpha}\tilde{\epsilon}\tilde{\Omega} \left(\frac{2k_B T}{E^2} - \frac{1}{E} \coth \frac{E}{2k_B T} \right), \quad (4)$$

$$B = \pi\tilde{\alpha} \left(\frac{2\tilde{\epsilon}^2 k_B T}{E^2} + \frac{\tilde{\Omega}^2}{E} \coth \frac{E}{2k_B T} \right) + \frac{\tilde{\Gamma}_{\text{out}}}{2}, \quad (5)$$

TABLE II. Mapping of the three-level approximation to a model with spinless electrons. The corresponding parameters for the detuning $\tilde{\epsilon}$, the tunnel coupling $\tilde{\Omega}$, the dot-lead rates $\tilde{\Gamma}_{\text{in,out}}$, and the dissipation strengths $\tilde{\alpha}$ and $\tilde{\alpha}'$ depend on the triple point at which the DQD is operated.

Three-level model	$\tilde{\epsilon}$	$\tilde{\Omega}$	$\tilde{\Gamma}_{\text{in}}$	$\tilde{\Gamma}_{\text{out}}$	$\tilde{\alpha}$	$\tilde{\alpha}'$
TP I	ϵ	Ω	$2\Gamma_L$	Γ_R	α	α'
TP II	ϵ	$\sqrt{2}\Omega$	Γ_L	Γ_R	α	$2\alpha'$
TP III	ϵ	Ω	Γ_R	$2\Gamma_L$	α	α'

and $E = (\tilde{\epsilon}^2 + \tilde{\Omega}^2)^{1/2}$ is the splitting of the one-electron states.

The corresponding stationary density operator and, thus, the corresponding current can be calculated analytically,

$$I = \frac{e}{\hbar} \frac{\tilde{\Omega}^2(2B - 4A_+\tilde{\epsilon}/\tilde{\Omega})}{4(\tilde{\epsilon}^2 + B^2) + \tilde{\Omega}^2 \left(\frac{4B+4(A_- - A_+)\tilde{\epsilon}/\tilde{\Omega}}{\tilde{\Gamma}_{\text{out}}} + \frac{2B-4A_+\tilde{\epsilon}/\tilde{\Omega}}{\tilde{\Gamma}_{\text{in}}} \right)} \quad (6)$$

$$\approx \frac{e}{\hbar} \frac{\tilde{\Omega}^2(\gamma - 2\pi\tilde{\alpha}\tilde{\epsilon})}{4\tilde{\epsilon}^2 + \gamma^2 + \tilde{\Omega}^2 \left(\frac{2\gamma}{\tilde{\Gamma}_{\text{out}}} + \frac{\gamma - 2\pi\tilde{\alpha}\tilde{\epsilon}}{\tilde{\Gamma}_{\text{in}}} \right)} \quad (7)$$

$$\approx \frac{e}{\hbar} \frac{\tilde{\Omega}^2(\gamma - 2\pi\tilde{\alpha}\tilde{\epsilon})}{4\tilde{\epsilon}^2 + (\gamma + 2\tilde{\Omega}^2/\tilde{\Gamma}_{\text{out}})\gamma}, \quad (8)$$

where $\gamma = \tilde{\Gamma}_{\text{out}} + 4\pi\tilde{\alpha}k_B T$. The approximation in Eq. (7) holds for sufficiently high temperature, such that in A_{\pm} and B , the hyperbolic cotangent becomes $\coth(E/2k_B T) \approx 2k_B T/E$. The final expression (8) holds if, in addition, $\tilde{\Gamma}_{\text{in}} \ll \gamma$, which in our setup is ensured by the fact that the emitter barrier is noticeably thinner than the collector's one.

B. Effective parameters

The mapping of our system to the Liouvillian (3) is achieved by two steps. First, one selects the three electron configurations, which may imply a summation over occupation probabilities for different spin configurations. Second, one relates the parameters of the full model to those of the spinless model, such that the current can be inferred from Eq. (8). The results are summarized in Table II. For all cases, we have verified numerically that in the relevant regime, the mapping represents a rather good approximation to the full description.

All triple points have in common that the coherent inter-dot tunneling connects two states which differ in the position of one electron. Therefore, the detuning ϵ has the same effect for all cases. Moreover, the transition matrix element of the dipole operator at all triple points agrees with the one of the spinless model. Hence, the dissipation strength of bath 1, which couples via the dipole operator, is the same in all cases, $\tilde{\alpha} = \alpha$.

1. Triple point I

Triple point I connects the empty DQD state and the occupation with one electron on the left or the right dot. Thus, the

situation comes close to the spinless case. The main difference is that an electron that arrives from the emitter may have any spin, such that the summation over the spin degree of freedom provides a factor 2 for the corresponding rate, $\tilde{\Gamma}_{\text{in}} = 2\Gamma_L$ (in a more formal treatment, one defines a probability $p = p_{\uparrow} + p_{\downarrow}$ [33]). For all subsequent transitions, including the dissipative ones, the spin is conserved such that all other parameters equal those of the spinless case.

2. Triple point II

At triple point II, the state with lowest occupation has one electron on the dot connected to the emitter. Owing to the Pauli principle, a second electron that tunnels to the left dot must have opposite spin. Therefore, no factor 2 emerges such that $\tilde{\Gamma}_{\text{in}} = \Gamma_L$. For the tunneling from the DQD to the collector, the situation is the same as at triple point I.

The more interesting issue is that the (1, 1) configuration may come as singlet or triplet, while in our model with one orbital per dot, the (2, 0) state is necessarily a singlet (the triplet state is higher in energy and, thus, is not accessible). Therefore, coherent tunneling occurs between the singlets $|\uparrow\downarrow, 0\rangle$ and $(|\uparrow, \downarrow\rangle + |\downarrow, \uparrow\rangle)/\sqrt{2}$. The corresponding matrix element of the inter-dot tunneling is $\sqrt{2}\Omega$, which can be identified with the tunneling in the spinless model. Dissipation in principle may cause leakage to a (1, 1) singlet, which would not be covered by our three-level model. In practice, however, these transitions do not play a role, because they are slower than the tunneling to the collector.

The factor $\sqrt{2}$ also occurs for the coupling to bath 2, which is established via the tunnel operator. Since the dissipative rates are proportional to the square of the transition matrix elements, one finds the correspondence $\tilde{\alpha}' = 2\alpha'$.

3. Triple point III

A striking feature of triple point III is that, in contrast to TP I and TP II, it is traversed counter-clockwise. Then the coherent inter-dot tunneling is initialized by the tunneling of an electron from the singly occupied right dot to the collector, such that we have the correspondence $\tilde{\Gamma}_{\text{in}} = \Gamma_R$. After the inter-dot tunneling, the system is reset by an electron tunneling from the left lead to the empty left dot. Hence, $\tilde{\Gamma}_{\text{out}} = 2\Gamma_L$. A shortcut to this reasoning can be established upon noticing that the situation can be interpreted as hole transport from the collector to the emitter. Then we are back to the situation at TP I, but with $\tilde{\Gamma}_{\text{in}}$ and $\tilde{\Gamma}_{\text{out}}$ interchanged.

4. Triple point IV

Let us finally remark that triple point IV is fundamentally different from the other three triple points, because emitter-DQD tunneling $(0, 1) \rightarrow (1, 1)$ may directly create a spin triplet which is not tunnel coupled to the $(0, 2)$ singlet. This

leads to Pauli spin blockade [34, 35] which can be lifted by dissipative processes such as spin dephasing or spin flips that may cause some residual currents. Such dissipative spin dephasing or spin flips, however, are fundamentally different from coherent inter-dot tunneling which dominates in the spinless model (and at the other triple points). Consequently, the dynamics at TP IV cannot be captured by a spinless model.

IV. Analytical expression for the background

To understand the action of bath 2, we focus on the regime aside the peaks in which the DQD eigenstates are well approximated localized states. There the bath coupling $H' = X \sum_{\nu} \lambda_{\nu} (b_{\nu}^{\dagger} + b_{\nu})$ with $X = \sum_{\sigma} (c_{L\sigma}^{\dagger} c_{R\sigma} + c_{R\sigma}^{\dagger} c_{L\sigma})$ induces dissipative transitions between states with different charge configuration, which enables transport. At triple point I, these configurations are (1, 0) and (0, 1). The transition rate can be calculated directly from Fermi's golden rule or by evaluating the corresponding terms of the master equation (2) and reads

$$\kappa_I(\epsilon) = \frac{\pi \alpha' \epsilon / \hbar}{1 - e^{-\epsilon/kT}}. \quad (9)$$

The expression is the product of the spectral density at the transition energy $\epsilon = E_{(1,0)} - E_{(0,1)}$ and the corresponding bosonic thermal occupation number. The resulting absorption rate follows formally by inverting the sign of the energy difference. Since κ_I is much smaller than the dot-lead rates $\Gamma_{L,R}$, the transitions induced by bath 2 represent the bottleneck of the transport process. Hence, the resulting current is approximately $I \sim e \kappa_I(\epsilon)$.

As discussed above, the tunnel matrix element between the singlets with charge configurations (2, 0) and (1, 1) augments the effective dissipative tunnel rate by a factor 2. Therefore, at triple point II, $I \sim e \kappa_{II}(\epsilon)$ with $\kappa_{II}(\epsilon) = 2 \kappa_I(\epsilon)$.

V. Additional spin flip noise

A Zeeman splitting enables additional dissipative processes such as spin flips. They may contribute to the resolution of the blockade mechanism at triple point I discussed in the main text. While a detailed investigation of this phenomenon is beyond the scope of the present work, we nevertheless provide some data to demonstrate that the role of spin flips may explain the discrepancy between theory and experiment at triple point I in the presence of a magnetic field.

We use a model similar to the one of ref. [36] with a bosonic bath that couples to one particular spin component. We choose the operator σ_x of each electron, which flips its spin. In second quantization, the corresponding system bath operator reads

$$V = \sum_{i=L,R} (c_{i\uparrow}^{\dagger} c_{i\downarrow} + c_{i\downarrow}^{\dagger} c_{i\uparrow}) \xi_i, \quad (10)$$

where the ξ_i is a Ohmic bath operator acting on the spin of dot i . They are defined as in the main text and have equal dimensionless coupling strength α_{spin} .

VI. Dephasing time of a charge qubit

The dissipative dynamics of a qubit possesses two characteristic times. While the population of the excited state decays during a relaxation time T_1 , coherent oscillations and interferences fade away exponentially on a time scale T_2 . For the Caldeira-Leggett model with only bath 1, i.e. for $\alpha' = 0$, both T_1 and T_2 can be obtained analytically and read [25, 26]

$$T_1^{-1} = \frac{\pi \alpha}{\hbar} \frac{\Omega^2}{E} \coth\left(\frac{E}{2kT}\right), \quad (11)$$

$$T_2^{-1} = \frac{1}{2} T_1^{-1} + \frac{\pi \alpha}{\hbar} \frac{2kT \epsilon^2}{E^2}, \quad (12)$$

with the energy splitting $E = \sqrt{\Omega^2 + \epsilon^2}$. In the high-temperature limit, $kT \gg E$, both times are proportional to the inverse temperature $1/T$, while they saturate at low temperature.

In principle, Eqs. (11) and (12) overestimate the coherence time of our charge qubit based on one- and two-electron states in a DQD as it uses a two-level approximation and neglects bath 2 and virtual transitions to the leads. To include the second bath, we consider the dissipative terms of our Bloch-Redfield master in the energy basis. This allows us to directly read off the decay rates of the populations and the coherences. In contrast to our transport calculations, we here disregard the dot-lead couplings and consider a qubit in a closed DQD configuration.

In Fig. S2 we compare the coherence time T_2 at triple point I as a function of temperature obtained from our master equation for various detunings. For the rather low value of α' in our setup, the result agrees almost perfectly with Eqs. (11) and (12). For temperatures larger than ~ 20 mK, we witness the $1/T$ behavior of the high-temperature limit.

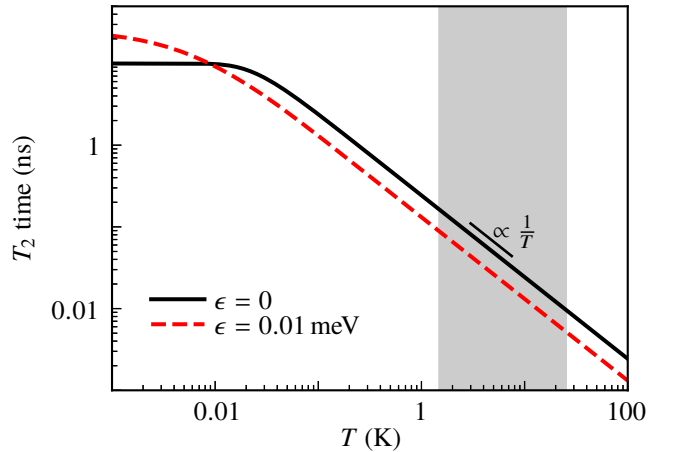


FIG. S2. Dephasing time T_2 of our model with the dimensionless dissipation strength determined in the main text. The values depict the inverse of the decay rate of the off-diagonal matrix element of the eigenstates that form the qubit at triple point I. All parameters are those determined by fitting to the current peaks in the main text. The grey area marks the temperature range of the experiment.